Trolley-Assisted Charging for Full-Shift Operation of Battery-Electric Load-Haul-Dump in Underground Mining

Lukas Gleisner J.[1], Diego Troncoso-Kurtovic[2], Ricardo Salas-Espiñeira[3], Jorge E. García Bustos[4], Bruno Masserano[5], Benjamín Brito Schiele[6], Francisco Jaramillo-Montoya[7], Heraldo Rozas[8], Ángela Flores-Quiroz[9], Luis F. Orellana[10,16], Jorge F. Silva[11], Gonzalo Monsalve[12], Gonzalo Ramírez[13], Marcos E. Orchard[14], and Javier Ruiz-del-Solar[15,17]

[1,2,3,4,5,7,8,9,11,14,15] *Department of Electrical Engineering, Faculty of Physical and Mathematical Sciences, University of Chile, Santiago, Chile*
lukas.gleisner@ug.uchile.cl
diego.troncoso.k@ug.chile.cl
ricardo.salas.e@ug.uchile.cl
jorgegarcia@ug.uchile.cl
bruno.masserano@ug.uchile.cl
francisco.jaramillo@uchile.cl
heraldo.rozas@ug.uchile.cl
angflores@uchile.cl
josilva@ing.uchile.cl
morchard@ing.uchile.cl
jruizd@ing.uchile.cl

[6] *Intelligent System Prognostics Group, Aerospace Structures and Materials Department, Faculty of Aerospace Engineering, Delft University of Technology, Delft, 2629HS, The Netherlands*
bbritoschiele@tudelft.nl

[10] *Departamento de Ingeniería en Minas, Facultad de Ciencias Físicas y Matemáticas, Universidad de Chile, Beauchef 850, Santiago, Chile*
luorella@uchile.cl

[12,13] *Corporación Nacional del Cobre de Chile (Codelco), Santiago, Chile*
gmons007@codelco.cl
grami018@codelco.cl

[16,17] *Advanced Mining Technology Center, Universidad de Chile, Santiago 837-0451, Chile*

ABSTRACT

Underground mining operations are transitioning to battery-electric fleets to reduce diesel emissions and ventilation requirements. However, current battery technology cannot sustain a full production shift in battery-electric load–haul–dump (LHD) vehicles, forcing mid-shift charging stops or battery swaps that disrupt production. Trolley-assisted systems (TAS) address this limitation by supplying external power along selected route segments through two complementary mechanisms: dynamic charging, in which an overhead catenary delivers energy while the vehicle travels, and static connection, in which the LHD connects to the trolley rail during brief scheduled stops, such as dumping. Together, these mechanisms reduce net battery discharge and extend battery autonomy without dedicated charging downtime. This paper presents a simulation-based framework to quantify the operating capability of TAS-equipped LHDs and evaluate trolley-length allocation at the production level. A physics-informed power and energy model, built on the Sandvik LH518iB architecture, is integrated into a route-level simulator that reproduces a full draw-control schedule on a real Chilean copper mine layout. The trolley length is treated as a configurable design parameter and systematically varied to assess its effect on battery autonomy, idle time, and throughput. Results show

that TAS can eliminate mid-shift battery swaps, improve productivity relative to battery-electric operation without TAS, and reduce energy cost per ton by up to 75% compared with diesel operation. Furthermore, route-to-route energy variability motivates a two-stage stochastic optimization framework to determine routing and charging strategies for a given trolley configuration.

1. INTRODUCTION

Underground mining operations still rely heavily on diesel-powered trackless mobile machinery, particularly for Load-Haul-Dump (LHD) cycles (Paraszczak, Svedlund, Fytas, & Laflamme, 2024). In confined underground environments, diesel-based fleets impose significant operational constraints because contaminants and heat must be continuously diluted and removed, making ventilation and cooling critical infrastructure (Halim, 2017). Ventilation is among the largest energy consumers in underground mines and directly links fleet composition to site-level energy demand and operating cost (Souza, 2015). These factors have intensified interest in electrification pathways that reduce ventilation requirements while maintaining productivity (Hooli & Halim, 2025).

In this context, Battery-Electric Vehicles (BEVs) are increasingly adopted because they eliminate tailpipe emissions, including diesel particulate matter, reduce heat and noise, and lower ventilation and air-conditioning burdens (Hooli & Halim, 2025). Despite these advantages, the main barrier to replacing diesel LHDs with battery-electric LHDs remains a technology-maturity limitation: current battery energy-storage and power-delivery capabilities are insufficient to support a full production shift. The energy-intensive duty cycles of underground LHD operations, characterized by steep grades, heavy payloads, and continuous stop-and-go behavior, deplete the onboard battery well before shift end, necessitating mid-shift charging or battery replacement. This constraint is consistently identified as the primary obstacle to large-scale adoption of battery-electric LHDs in underground mining (Global Mining Guidelines Group (GMG), 2022).

Because the onboard energy budget is depleted before shift completion, operations must rely on complementary charging strategies, such as in-shift fast charging, opportunity charging during unavoidable idle periods, or battery swapping, to close the energy gap. Each option entails nontrivial infrastructure and operational requirements, including power distribution, charging-station layout, scheduling and queueing constraints, safety considerations, and system interoperability.

Current underground electrification solutions can be grouped into three approaches: battery swapping, fast charging, and trolley-assisted systems (TAS). Battery swapping can reduce charging downtime by replacing depleted packs with charged ones at a dedicated battery swapping station (BSS), decoupling charging duration from vehicle operation and enabling replenishment within minutes (Alhazmi, 2025; Sarker, Pandžić, & Ortega-Vazquez, 2014). Prior work reports that swapping reduces waiting times relative to plug-in charging and improves service availability (Ahmad, Saad Alam, Saad Alsaidan, & Shariff, 2020), while centralized BSS operation supports structured charging schedules, battery health monitoring, and potential degradation mitigation compared with repeated fast charging at the production level (Alhazmi, 2025; Vani, Kishan, Ahmad, & Reddy, 2024). However, battery swapping entails significant capital cost, as the battery pack is the most expensive vehicle component. A swapping-based strategy requires at least two full packs per vehicle (one in operation and one charging at the station), effectively doubling battery investment (Wu, 2021; Alhazmi, 2025). Beyond cost, large-scale deployment is hindered by the need for dedicated infrastructure, including automated handling systems, safety equipment, and significant space requirements (Wu, 2021; Alhazmi, 2025). In underground mining environments, these spatial requirements may make battery-swapping bays infeasible or prohibitively expensive, as available space is inherently limited and additional excavation may compromise the long-term geomechanical stability of the mine. Battery logistics and inventory management further increase operational complexity (Hooli, Skawina, Halim, & Sundqvist, 2024), while limited standardization across manufacturers constrains cross-brand usability (Alhazmi, 2025). Each swap event also removes the vehicle from production, reducing equipment availability; when multiple swaps per shift are required, cumulative downtime can significantly reduce throughput (Ahmad et al., 2020).

Fast charging refers to off-board, high-power EV charging, typically DC fast charging (DCFC) and ultra-fast charging (UFC), in which energy is delivered directly to the battery at power levels of 50–100 kW, enabling substantial State-of-Charge (SoC) recovery within tens of minutes (Zentani, Almaktoof, & Kahn, 2024; Mojlish, Sutanto, & Muttaqi, 2025). Mature, standardized interfaces (e.g., CCS, CHAdeMO) support scalable infrastructure deployment (Sawant & Zambare, 2024). However, in underground mining, fast charging presents important drawbacks: repeated high-C-rate charging accelerates battery degradation through increased thermal stress (Zentani et al., 2024), and each charging event removes the vehicle from production. Moreover, high-power charging stations impose significant demands on the mine electrical network and may introduce power-quality issues that require grid reinforcement or local energy storage (Muttaqi, Isac, Mandal, Sutanto, & Akter, 2024; Mojlish et al., 2025).

Finally, TAS are an electrification approach in which vehicles draw electrical power from overhead catenary lines through a pantograph while operating on specific road segments (Valenzuela Cruzat & Valenzuela, 2018). TAS can supply energy through two complementary mechanisms. The first is dynamic charging, in which the LHD draws power

from the overhead catenary while traveling along an electrified segment, enabling direct grid-powered traction and simultaneous battery charging during operation (Wei, Liu, Liu, & Feng, 2025). The second is static connection, in which the vehicle connects to the trolley rail during a brief scheduled stop, for example, while dumping material, enabling concentrated energy transfer without a dedicated charging station or additional downtime. Together, these mechanisms reduce net battery discharge per cycle and extend operational autonomy without removing the vehicle from production.

The literature identifies TAS as an effective means of alleviating the energy-density limitations of onboard batteries by reducing stationary charging requirements, enabling smaller battery sizes, and improving duty-cycle performance and productivity, particularly in energy-intensive applications such as surface mining haulage (Bao, Knights, Kizil, & Nehring, 2024, 2025). Quantitative studies report benefits, including higher uphill speeds, shorter cycle times, lower fuel or onboard energy consumption, and lower lifecycle greenhouse gas emissions than those of diesel-electric or battery-only alternatives (Valenzuela Cruzat & Valenzuela, 2018; Wei et al., 2025). In addition, supplying traction power directly from the grid can reduce sustained high battery C-rate operation and may mitigate battery degradation relative to aggressive fast-charging strategies (Wei et al., 2025). Compared with battery swapping, TAS avoids duplicate battery packs and the associated capital cost while improving equipment availability by eliminating swap-related downtime. However, TAS requires fixed infrastructure investment, including overhead lines, substations, and power electronics (Valenzuela Cruzat & Valenzuela, 2018), and its benefits are limited to equipped road segments (Bao et al., 2025). System performance also depends on coordination among trolley availability, fleet size, and mine or route planning, as limited access to trolley lines can create bottlenecks and underutilization (Bao et al., 2025). Overall, trolley assistance is effective but context-specific, motivating hybrid BEV LHD designs that combine onboard batteries with optimally allocated trolley segments.

In such hybrid configurations, dynamic charging delivers energy along strategically selected segments while the vehicle is in motion, and static connections provide additional energy during brief scheduled stops, together extending effective autonomy and reducing reliance on dedicated stationary charging during production. The onboard battery preserves full-network coverage and operational flexibility. Under this hybrid paradigm, the key design question is no longer whether TAS should be used, but how limited trolley infrastructure should be allocated and integrated to enable uninterrupted full-shift LHD operation.

A critical gap remains in the development of formal criteria and decision-support tools to quantify the energy autonomy of hybrid TAS-assisted BEV LHD fleets under high-fidelity production schedules. While the benefits of TAS are well recognized, existing research lacks methods to verify whether a given infrastructure configuration, characterized by total trolley length and charging power, can satisfy shift-length requirements without mid-shift recharging or battery replacement. This limitation is compounded by the lack of integrated frameworks for the spatial and operational design of trolley infrastructure. In particular, there is no established approach for optimizing the allocation of a given trolley length at the production level or determining the appropriate balance between dynamic charging segments and static connection intervals. As a result, current assessments often remain qualitative, and identifying the infrastructure configuration required to ensure uninterrupted operation remains an open challenge for the large-scale underground deployment of electrified fleets. While related work by the authors introduced stochastic characterization of LHD operational profiles (Gleisner et al., 2025), no prior publication addresses this system-level design problem. The physics-informed power-and-energy model employed in this paper was developed and validated in separate ongoing work and is used here as the computational core of the proposed framework.

This paper presents a simulation-based framework to assess and design TAS for battery-electric LHDs in large-scale underground mining, aiming to ensure full-shift energy autonomy without production interruptions. Total trolley length is treated as a configurable design parameter and systematically varied to assess its effects on autonomy, idle time, and throughput, while optimization determines routing and charging decisions for each configuration.

The proposed framework operates as an operational health-management layer for battery-electric fleets: the State of Energy (SoE) trajectory serves as a proxy health indicator that couples battery condition awareness with routing and charging decisions. Maintaining the SoE within safe bounds and balancing utilization across packs are health-preserving objectives, so the throughput and downtime metrics reported here are fleet-level health-management outcomes rather than purely productivity indicators.

The main contributions of this work are:

- A route-level simulation environment for realistic evaluation of production rate and cycle time on a real underground mine layout under a draw-control schedule, constituting the first framework of this kind applied to TAS-assisted BEV LHD fleets.
- A systematic evaluation of parametric TAS configuration scenarios in which total trolley length is treated as a configurable design parameter and varied across multiple configurations, including both dynamic trolley segments and static connection intervals, to formally quantify effects on energy autonomy, operational feasibility, and production continu-

ity. This addresses a gap in the literature where such assessments have remained qualitative.

- A comparative assessment against battery-only and diesel baselines, quantifying autonomy and productivity metrics, and identifying optimized routing and charging strategies for predefined TAS configurations through the proposed optimization framework, providing decision-support criteria for infrastructure sizing currently absent from the state of the art.

Section II introduces the autonomy and modeling foundations of this study; Section III describes the experimental setup, including the physics-informed model, route-level simulation framework, and stochastic optimization formulation; Section IV presents the optimization results and comparative assessment; and Section V concludes the paper and outlines future research directions.

2. THEORETICAL BACKGROUND

This section introduces the theoretical foundations of the simulation-based autonomy assessment developed in Section 3. In particular, it defines an energy-domain battery state variable suitable for shift-level evaluation and summarizes the main principles of electromechanical modeling for battery-electric LHDs. These foundations link operational cycles (haul, dump, return) and route constraints to battery power demand, which is later used to estimate autonomy under trolley-assisted operation.

2.1. State of Energy (SOE)

Battery autonomy in underground mining is governed by the energy balance accumulated over repetitive operational LHD duty cycles. During a production shift, the battery is subjected to highly variable power demand driven by haulage ramps, payload changes, stop-and-go behavior, and auxiliary loads. Under these conditions, an energy-based state variable provides a direct measure of the remaining energetic margin available to sustain traction and auxiliary requirements.

The State of Energy (SOE) is commonly defined as the ratio between the remaining usable energy and a reference maximum usable energy:

$$\mathrm{SoE}(t) = \frac{E_{\mathrm{rem}}(t)}{E_{\max}}, \tag{1}$$

where $E_{\mathrm{rem}}(t)$ denotes the remaining usable energy at time t, and $E_{\max}$ is the maximum usable energy under the adopted operating assumptions (e.g., voltage bounds and admissible power limits) (He, Zhang, Xiong, & Wang, 2015; Liu, Wu, Zhang, & Chen, 2014).

A practical model for SoE is obtained from the battery electrical power balance. Using the sign convention $P_{\mathrm{bat}}(t) > 0$ during discharge and $P_{\mathrm{bat}}(t) < 0$ during charging, the remaining energy evolves as:

$$E_{\mathrm{rem}}(t) = E_{\mathrm{rem}}(t_0) - \int_{t_0}^{t} P_{\mathrm{bat}}(\tau)\, d\tau. \tag{2}$$

This formulation directly supports route-based evaluation by naturally incorporating both energy expenditure and energy recovery/supply events (e.g., regenerative braking or trolley charging) (Rozas, Troncoso-Kurtovic, Ley, & Orchard, 2021).

2.2. Markov-Chain Velocity Model

Vehicle velocity profiles in stochastic environments can be modeled using Markov chains, which provide a probabilistic framework for sequential processes. A discrete-time Markov chain is defined by a finite set of states and a transition probability matrix $\mathbf{P}$, where each element P_{ij} represents the probability of transitioning from state i to state j. In its classical form, the evolution of the system is given by:

$$\mathbb{P}(X_{k+1} = j \mid X_k = i) = P_{ij}, \tag{3}$$

which satisfies the Markov property, whereby the future state depends only on the current state (Zhao, Li, Zhao, Ke, & Wang, 2022).

In this work, the transition dynamics are extended to include state-dependent variables. Specifically, the Markov chain is conditioned on the vehicle's velocity v_k, acceleration a_k, and cumulative distance d_k, yielding:

$$\mathbb{P}(X_{k+1} = j \mid X_k = i, v_k, a_k, d_k), \tag{4}$$

where X_k represents the discrete acceleration state at time step k (acceleration, deceleration, or constant speed). This formulation defines a non-homogeneous, context-dependent Markov process in which transition probabilities vary with the current operating conditions.

While the Markov chain governs the evolution of discrete acceleration states, the acceleration magnitude within each state is modeled as a continuous stochastic variable. Specifically, the acceleration is sampled from a conditional distribution:

$$a_k \sim f(a \mid v_k), \tag{5}$$

where $f(\cdot)$ is an empirical distribution derived from operational data.

The continuous vehicle dynamics are obtained by embedding this stochastic process in a state-space model based on Newtonian mechanics:

$$v_{k+1} = v_k + a_k \Delta t, \tag{6}$$

$$x_{k+1} = x_k + v_k \Delta t + \frac{1}{2} a_k \Delta t^2, \tag{7}$$

where v_k and x_k denote the velocity and position at time step

k, respectively, and Δt is the sampling interval of the sample acceleration distribution.

This hybrid formulation, combining a context-dependent Markov process with a continuous state-space model, enables the generation of stochastic velocity trajectories that capture both the probabilistic nature of driving behavior and the underlying vehicle dynamics. By repeatedly sampling from transition probabilities and conditional acceleration distributions, a large number of possible trajectories can be generated via Monte Carlo simulation, enabling exploration of feasible operating conditions and statistical characterization of system behavior under uncertainty (Gleisner et al., 2025).

2.3. Electromechanical Modelling

Electromechanical modeling refers to the development of a physics-consistent, control-oriented representation of a vehicle that couples its mechanical motion to the electrical power-conversion processes that supply traction. For a battery-electric LHD operating underground, the purpose of this modeling framework is to reproduce, with sufficient fidelity, the vehicle response over repetitive operational cycles (haul-dump-return) and to estimate the instantaneous battery electrical power demand throughout an entire shift. The resulting battery power trajectory provides the required input to energy-domain autonomy calculations (cf. Section 2.1).

In an electromechanical model, the longitudinal dynamics are driven by a force balance of the form (Guzzella & Sciarretta, 2007; Larminie & Lowry, 2012):

$$m\dot{v}(t) = F_{\mathrm{trac}}(t) - F_{\mathrm{res}}(t), \tag{8}$$

where m is the LHD mass, defined as m_{veh} (unloaded) or $m_{\mathrm{veh}}+m_{\mathrm{payload}}$ (loaded), v is the longitudinal speed, F_{trac} is the traction force delivered at the wheels, and F_{res} represents the aggregated resistive forces. In underground hauling, F_{res} is commonly dominated by grade-related components during ramp ascent/descent, rolling resistance, and speed-dependent drag, and can be expressed as:

$$F_{\mathrm{res}}(t) = mg\sin\theta(t) + C_{rr}mg\cos\theta(t) + \frac{1}{2}\rho A C_d v^2(t), \tag{9}$$

where $\theta(t)$ is the route grade, C_{rr} is the rolling resistance coefficient, ρ is air density, and A and C_d represent the reference area and drag coefficient, respectively. Vehicle dimensions and configuration influence both A and the equivalent resistive terms, and are therefore relevant parameters in realistic LHD modeling (Larminie & Lowry, 2012; Guzzella & Sciarretta, 2007).

Traction force is generated from wheel torque:

$$F_{\mathrm{trac}}(t) = \frac{T_{\mathrm{wheel}}(t)}{r_{\mathrm{wheel}}}, \tag{10}$$

where r_{wheel} is the effective wheel radius. Wheel torque is linked to motor torque through the driveline, which typically includes gearbox reduction and mechanical losses:

$$T_{\mathrm{wheel}}(t) \approx \eta_{\mathrm{drv}}\, G\, T_{\mathrm{motor}}(t), \tag{11}$$

with G the gear ratio and η_{drv} the drivetrain efficiency. In practice, driveline modeling may also incorporate inertias and compliance, which influence torque transients and therefore impact power peaks and energy consumption over short intervals (Guzzella & Sciarretta, 2007).

A defining characteristic of electromechanical modeling is the explicit inclusion of the control layer and its dynamic response. Rather than assuming instantaneous torque delivery, the commanded traction is mediated by nested control loops (e.g., speed tracking and torque/current regulation) that can be approximated by transfer functions or state-space representations. A standard conceptual structure is:

$$v_{\mathrm{ref}}(t) \xrightarrow{\mathcal{C}_v(s)} T_{\mathrm{ref}}(t) \xrightarrow{\mathcal{C}_T(s)} T_{\mathrm{motor}}(t), \tag{12}$$

where $\mathcal{C}_v(s)$ and $\mathcal{C}_T(s)$ denote the outer speed controller and inner torque/current controller, respectively. This representation enables modelling realistic tracking performance and actuator limitations, including saturation constraints such as:

$$|T_{\mathrm{motor}}(t)| \le T_{\max}\big(\omega_{\mathrm{motor}}(t)\big),\ |P_{\mathrm{mech}}(t)| \le P_{\max}, \tag{13}$$

which are critical for heavy-duty mining cycles where torque demand can remain high for sustained ramp segments.

Furthermore, realistic traction modeling must account for tire–ground interaction phenomena, particularly tire slip. Under low-adhesion conditions (dust, wet ground, uneven surfaces) or high torque requests, the longitudinal traction force may be limited by friction and slip dynamics. A common approach is to compute traction as a function of slip ratio κ using empirical tire models (Pacejka, 2005):

$$F_{\mathrm{trac}}(t) = f\big(\kappa(t), F_z(t)\big), \tag{14}$$

where F_z is the normal load. In an electromechanical simulation, incorporating slip is important because it constrains achievable acceleration and can increase losses and energy expenditure, especially in aggressive transients or ramp hauling.

where η_{elec} represents the aggregated efficiency of the inverter–motor system and P_{aux} captures non-traction loads relevant to the LHD (e.g., thermal management, onboard electronics, and auxiliary subsystems) (Larminie & Lowry, 2012; Guzzella & Sciarretta, 2007). Because $P_{\mathrm{bat}}(t)$ is computed at each time step of the cycle, the electromechanical model provides a high-resolution representation of how route geometry, payload-dependent resistance, drivetrain limits, and control actions translate into battery energy depletion

over the shift. Consequently, autonomy can be evaluated in a physically consistent manner by integrating $P_{\text{bat}}(t)$ within the SoE dynamics.

3. METHODOLOGY

The overall methodological framework adopted in this work is illustrated in Figure 1, which integrates data-driven modeling, physical system representation, and stochastic optimization for decision-making under uncertainty.

3.1. Stochastic Optimization

Based on the preliminary analysis presented in the following section, an optimization framework is required to properly determine the routes to be taken, particularly along segments where energy regeneration occurs. To accurately reflect the operational capabilities of the electric LHD, the operating strategy must be rigorously optimized while accounting for range limitations and charging logistics. Accordingly, a two-stage stochastic optimization model was developed to govern routing and battery-replacement decisions, ensuring robustness to uncertainty in energy consumption in underground environments. In this preliminary study, the trolley system configuration, namely rail length and substation power, is treated as configurable design parameters and systematically varied to assess their impact on system performance. The primary objective is to test the hypothesis that optimization is necessary to fully exploit the system's operational capabilities. This allows operational decisions to be optimized without prematurely addressing infrastructure design. Joint optimization of infrastructure sizing and operation is therefore left for future work, once the need for an optimization-based operating strategy has been validated.

The mathematical formulation begins by defining the operational domain and the associated parameters, which are summarized in Table 1. The numerical values of the cost coefficients are not explicitly specified, as they depend on the internal economic conditions of each mining operation. Instead, the model relies on the relative magnitude of these coefficients to guide the optimization. In particular, the cost structure is defined such that energy injection via opportunity charging is always preferred when feasible, whereas battery swapping occurs only when no viable charging alternative is available.

Although the cost values are not explicitly quantified, battery swapping is intentionally assigned a high relative cost. This reflects the substantial capital and operational effort required to implement swapping infrastructure in underground environments, where space constraints and existing mine layouts are not typically designed to accommodate dedicated swapping bays. In practice, these spatial limitations may make such installations infeasible or excessively costly. Furthermore, battery packs constitute one of the most significant capital expenditures in electric mining operations. Accordingly, strategies that reduce the number of batteries required (ideally to fewer than two per vehicle) are inherently favored within the proposed framework, as they directly reduce both capital requirements and operational complexity. This also justifies the additional capital investment associated with TAS infrastructure, as in-route energy injection reduces reliance on bat-

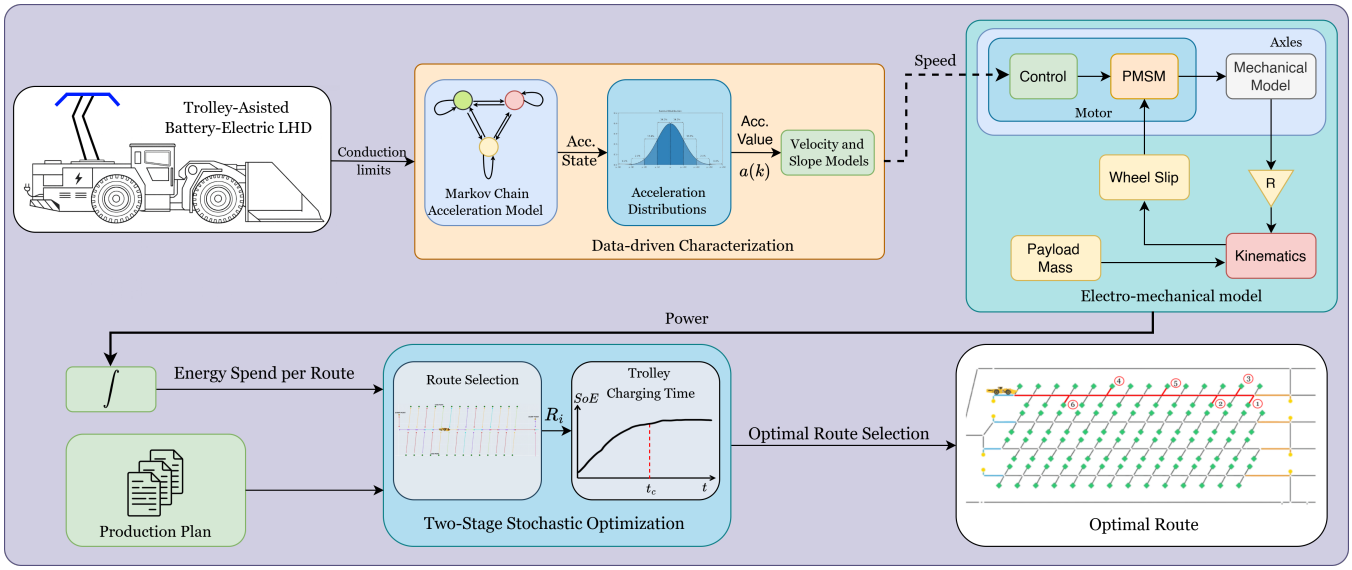

Figure 1. Overall methodological framework of the proposed approach. The pipeline integrates data-driven characterization of vehicle dynamics, electro-mechanical modeling, and a two-stage stochastic optimization model for route and energy management under uncertainty.

Table 1. Sets, parameters, and decision variables of the optimization model.

Symbol	Description	Index / Unit
Sets and indices		
$\mathcal{B}$	Batteries	b
$\mathcal{R}$	Feasible routes	r
$\mathcal{R}_f \subseteq \mathcal{R}$	Feasible routes associated with extraction point f	r
$\mathcal{C} = \{1, \ldots, N\}$	Operating working cycles	c
$\mathcal{F}$	Extraction points	f
Parameters		
$P_{trolley}$	Trolley power	kW
L_{Rail}	Trolley rail length	m
$E^{\max}$	Maximum battery energy	kWh
$E^{\min}$	Minimum battery energy	kWh
E_b^0	Initial energy of battery b	kWh
$\xi_{b,r}^{\omega}$	Energy consume on route r by battery b in scenario ω	kWh
N_{swap}	Maximum number of swaps allowed	–
$t^{\max}$	Maximum waiting time per cycle	h
t^{dump}	Dumping time per cycle	h
η	Battery efficiency	–
C_S	Cost per swap event	USD/swap
C_{kWh}	Cost of energy inyection	USD/kWh
M^W	Upper bound on total waiting energy	–
Decision variables		
$x_{r,c}$	Selection of route r in cycle c	binary
$a_{f,c}$	Visit to extraction point f in cycle c	binary
s_c	Swap occurrence in cycle c	binary
$E_{b,c}$	Energy of battery b at the beginning of cycle c	kWh
$E_{b,c}^W$	Energy obtained through waiting in cycle c	kWh
$E_{b,c}^D$	Energy obtained through out the dumping in cycle c	kWh
$U_{b,c}$	Linearization of $s_c E_{b,c}$	kWh

tery swapping and, consequently, the total battery capacity at the fleet level.

The objective function, defined in Eq. (15), minimizes the expected total operational cost. This cost comprises two main components: the cost associated with battery replacement events (swaps), C_S, and the cost of energy injection C_{kWh}. The latter is further divided into two terms. Energy obtained during idle waiting is assigned a higher penalty to prioritize energy injection during load dumping, since this does not reduce productive time. Investment costs associated with installing the trolley infrastructure are not included, as this formulation focuses solely on the operational stage.

$$\min \quad C_S \sum_{c\in\mathcal{C}} s_c + C_{kWh} \sum_{\omega\in\Omega} \alpha_\omega \left[2 \sum_{b\in\mathcal{B}} \sum_{c\in\mathcal{C}} E_{b,c}^{W,\omega} + \sum_{b\in\mathcal{B}} \sum_{c\in\mathcal{C}} E_{b,c}^{D,\omega} \right] \tag{15}$$

The optimization is subject to a set of operational and physical constraints. Regarding the first-stage decisions, Eqs. (16) through (20) enforce the logistical logic of the mining process. Specifically, exactly one route must be selected per cycle (Eq. (16)), and the vehicle must be assigned to exactly one extraction point per cycle (Eq. (17)). Let $\mathcal{R}_f \subseteq \mathcal{R}$ denote the subset of feasible routes associated with extraction point f. The selected route must be consistent with the assigned extraction point, as enforced by Eq. (18). Furthermore, the total visits to each extraction point must match the scheduled demand N_f (Eq. (19)), and due to geomechanical constraints, the vehicle is restricted from visiting the same extraction point for more than three consecutive cycles (Eq. (20)).

$$\sum_{r\in\mathcal{R}} x_{r,c} = 1, \quad \forall c \in \mathcal{C} \tag{16}$$

$$\sum_{f\in\mathcal{F}} a_{f,c} = 1, \quad \forall c \in \mathcal{C} \tag{17}$$

$$\sum_{r\in\mathcal{R}_f} x_{r,c} = a_{f,c}, \quad \forall f \in \mathcal{F},\ c \in \mathcal{C} \tag{18}$$

$$\sum_{c\in\mathcal{C}} a_{f,c} = N_f, \quad \forall f \in \mathcal{F} \tag{19}$$

$$\sum_{i=0}^{3} a_{f,c+i} \le 3, \quad \forall f \in \mathcal{F}, c = 1, \ldots, N-3 \tag{20}$$

Additionally, the total number of battery replacements permitted over the entire horizon is bounded by N_{swap}, as enforced by Eq. (21):

$$\sum_{c\in\mathcal{C}} s_c \le N_{swap} \tag{21}$$

The second-stage constraints govern the system's energy dynamics for each scenario. The evolution of the SoE is described by the balance equation in Eq. (22), which updates the battery energy for the subsequent cycle based on the current energy, the energy gained during dumping and waiting periods, the energy replenished through battery swapping, and the energy consumed while traversing the selected route. The consumption term $\xi_{b,r}^{\omega}$ is obtained from the scenario-dependent energy models described previously. The route scenarios are defined using the 10th, 30th, 50th, 70th, and 90th percentiles in order to capture both extreme and representative operating conditions, while also enabling a direct comparison with the preliminary study.

$$E_{b,c+1}^{\omega} = E_{b,c}^{\omega} + E_{b,c}^{W,\omega} + E_{b,c}^{D,\omega} + E^{max} s_c - U_{b,c}^{\omega} - \sum_{r\in\mathcal{R}} \xi_{b,r}^{\omega} x_{r,c} \quad \forall b \in \mathcal{B}, \forall c = 1, \ldots, N-1, \forall \omega \in \Omega \tag{22}$$

The feasible operation of the battery and the charging system is constrained by Eqs. (23), (24), and (25), which limit the SoE to the battery's capacity, the dumping and wait time charging to the maximum power transfer capability of the trolley connection, respectively.

$$E^{\min} \le E_{b,c}^{\omega} \le E^{\max} \tag{23}$$

$$0 \le E_{b,c}^{D,\omega} \le t^{dump} \eta P_{trolley} \tag{24}$$

$$0 \le E_{b,c}^{W,\omega} \le t^{max} \eta P_{trolley} \tag{25}$$

To preserve the linearity of the model while accounting for the conditional reset of energy during a battery swap, the bilinear term $s_c E_{b,c}^{\omega}$ in the balance equation is replaced by the

auxiliary variable $U^{\omega}_{b,c}$. This variable is constrained by the McCormick envelopes presented in Eqs. (26) through (29), which ensure that $U^{\omega}_{b,c}$ correctly represents the energy remaining in the battery at the moment of a swap.

$$U^{\omega}_{b,c} \leq E^{max} s_c \tag{26}$$

$$U^{\omega}_{b,c} \leq E^{\omega}_{b,c} \tag{27}$$

$$U^{\omega}_{b,c} \geq E^{\omega}_{b,c} - E^{max}(1 - s_c) \tag{28}$$

$$U^{\omega}_{b,c} \geq 0 \tag{29}$$

Finally, to ensure the technical feasibility of the substation supplying the trolley system, Eq. (30) imposes an upper bound on the total cumulative energy that can be drawn during waiting periods across all cycles and batteries for each scenario.

$$\sum_{b \in \mathcal{B}} \sum_{c \in \mathcal{C}} E^{W,\omega}_{b,c} \leq M^W E^{max}, \quad \forall \omega \in \Omega \tag{30}$$

This constraint effectively limits the total waiting time and prevents the operational strategy from relying excessively on idle charging. The optimization problem was solved as a mixed-integer linear program (MILP) using Gurobi, implemented with the default solver settings on an Intel i9-13900K processor.

4. RESULTS

4.1. Case Study

To conduct this case study, a hybrid data-driven and physics-based framework was developed to model the battery power consumption of an electric LHD. The stochastic characterization of vehicle operation was derived from operational data collected during an electric LHD pilot at El Teniente Division, Bajo Diablo Regimiento (Chile). Driving behavior was modeled using a unified framework that combines clustering techniques with a context-dependent Markov chain. Specifically, acceleration and braking signals were analyzed using dynamic time warping (DTW) and fuzzy clustering to group cycles with varying durations into a set of representative operational modes, which define state-dependent transition probabilities between acceleration regimes (acceleration, deceleration, and constant speed). These transitions are conditioned on the vehicle's previous velocity and acceleration, as well as the cumulative distance traveled.

Acceleration magnitudes were sampled from empirical distributions estimated from the data, while operational constraints, such as speed limits, geometric constraints (e.g., curves), and loading events, were enforced. This stochastic framework enables the generation of multiple feasible trajectories via Monte Carlo simulation, as detailed in previous work (Gleisner et al., 2025).

The resulting velocity profiles were then used as inputs to a physics-based model derived from the technical specifications of the Sandvik LH518iB. This model explicitly incorporates the main vehicle subsystems, including the number, characteristics, and configuration of the electric motors, battery connection topology, vehicle dimensions, torque requirements, power electronics, and control-loop dynamics. Furthermore, operational data are used to provide a stochastic representation of peak-power events associated with bucket operation. Specifically, these events are modeled using two empirical distributions: one describing the number of peak events per cycle and another characterizing the energy demand of each event. In addition, the energy requirements associated with bucket loading and unloading are directly characterized from the operational data, allowing the model to capture the transient dynamics of these processes. The model also accounts for variations in vehicle mass by updating the payload at loading events, ensuring consistency with typical mining conditions. Due to the lack of detailed measurements for auxiliary loads, such as air conditioning, steering hydraulics, and onboard electronic systems, a constant power consumption of 4 kW is assumed. It is important to note that this auxiliary term does not include bucket operation, which is modeled separately as a stochastic peak-power event, as described above.

The total energy consumption associated with a given extraction point is defined as the sum of traction, bucket operation, and auxiliary energy components:

$$E_{\text{cons}} = E_{\text{trac}} + E_{\text{lift}} + E_{\text{unload}} + E_{\text{aux}}, \tag{31}$$

where E_{trac} corresponds to the energy expended in traction, E_{lift} is the energy required for bucket lifting, E_{unload} represents the energy consumed during bucket unloading, and E_{aux} accounts for auxiliary loads.

To ensure the reliability of the simulation results, the model was validated against manufacturer-provided speed and acceleration data and against independent third-party studies.

Using the validated model, a full-day production schedule (draw-control schedule), equivalent to 240 cycles and based on a mean payload of 15.3 t, was simulated to estimate the hourly tonnage of the electric LHD operating on a route layout derived from Sector N21 of the Chuquicamata Mine (Calama, Chile), where the production requirements correspond to the demand of Street C1. Although the layout is representative of realistic operating conditions, this sector of the mine is currently under development. The layout is shown in Figure 2. TAS infrastructure was implemented along selected route segments, specifically at the dumping zones, with a maximum electrified length of 26.5 m. This length was selected as the maximum safe span for rail installation, allowing dynamic power injection while the vehicle is in motion. Consequently, net energy consumption per cycle is reduced, increasing vehicle operational autonomy. The proposed frame-

work is not restricted to this layout and can be adapted to any underground mine given sufficient information on route geometry, production schedule, and operational parameters.

To ensure a realistic representation of the working cycle, defined as traveling to the extraction point and subsequently dumping at the dumping point, a dumping time of 10 s was assumed. This interval corresponds to effective production time, as it is required for normal operation; therefore, energy injection during this period does not affect productivity. Consequently, the vehicle was assumed to be charged while positioned at the dumping point, enabling more efficient use of the trolley infrastructure. Furthermore, to account for the inherent variability of individual cycles, the mean velocity profile and mean payload were used to estimate total daily energy expenditure.

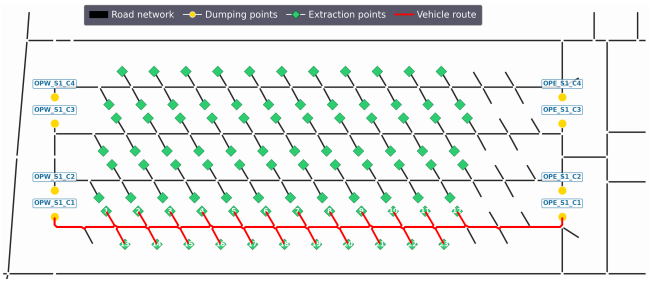

Figure 2. Layout of the simulation derived from Sector N21 of the Chuquicamata Mine (Calama, Chile), indicating production points (shown in green), dumping point (shown in yellow), and segments equipped with TAS infrastructure (shown in blue and orange). Although the layout is representative of realistic operating conditions, this sector of the mine is currently under development and not yet fully operational.

For comparative purposes, the performance of a conventional diesel-powered LHD was estimated using baseline operational data. The comparison was conducted based on throughput, which was selected as the reference indicator, given that diesel vehicles generally operate at lower maximum speeds than their electric counterparts.

4.2. Preliminary Study

As described in the methodology section and as justification for the study presented in this article, the preliminary analyses indicate that an optimization strategy is required to ensure efficient use of the available energy. Furthermore, these analyses suggest that the implementation of TAS is technically and economically feasible.

Results are summarized in Table 2, which reports the performance obtained for different trolley rail lengths and charging power levels. A moderate charging rate of 0.5 C is used to demonstrate that, even when operating below the maximum charging capacity, the proposed model can identify solutions that substantially improve operational performance. In addition, a dumping time of 10 s is assumed, during which the LHD can be charged without interfering with the production cycle. This is consistent with conventional LHD operating practice and therefore represents a realistic opportunity-charging period rather than an idealized condition.

To formalize the energy balance at the cycle level, the net energy consumption per extraction point is defined as

$$E_{\text{net}} = E_{\text{base}} - E_{\text{dump}} - E_{\text{static}}, \tag{32}$$

where E_{base} represents the baseline energy consumption, E_{dump} is the energy injected during the dumping phase, and E_{static} corresponds to the energy supplied during static waiting periods.

To evaluate the system's sensitivity to charging power, an additional scenario with a 10% increase in charging capacity was analyzed. The results reveal a clear relationship between trolley rail length and the corresponding increase in vehicle autonomy. Moreover, charging power has a key, distinctly non-linear influence on system performance. In particular, a 10% increase in charging capacity can lead to a reduction in idle time of up to 100%, highlighting the strong leverage of charging power within the proposed framework.

Moreover, as shown in Table 2, a secondary decision variable can further improve system performance: the static time. This variable emerges not only as an alternative mechanism to extend vehicle autonomy without increasing the trolley rail length, but also as a particularly relevant strategy, given that the zones where the trolley infrastructure should be installed are highly hazardous. Consequently, reducing the required trolley length while preserving autonomy has clear operational and safety benefits.

The inclusion of a static waiting time introduces an equivalence between different trolley rail lengths, as shown in Table 2, where comparable autonomy levels are achieved through different combinations of rail length and waiting time. Note that, in this case, the idle time equals the sum of the battery-swap duration (0.33 h) and the total waiting time.

This observation reveals a trade-off between trolley infrastructure deployment and operational waiting strategies. In the present work, however, the trolley rail length is treated as a fixed parameter, and the optimization is therefore restricted to operational decisions for a given infrastructure configuration. The joint optimization of rail length and operational strategy remains a promising direction for future research.

Although the results provide a preliminary indication of the feasibility and potential benefits of trolley-assisted operation, they already demonstrate that, for certain trolley lengths, the vehicle can complete a full working day without a battery swap, thereby avoiding the complex maneuvers and operational requirements associated with battery swaps. Moreover,

Table 2. Operational performance for different trolley lengths and static charging times during a typical day of operation under two charging strategies (charging power expressed in C-rate). Throughput gain is computed relative to the diesel baseline. All trolley scenarios include energy injection during the dumping phase by default, while any additional charging from static time is applied after this period.

Trolley rail (m)	Static (s)	Total operational time (h)	Idle (h)	Battery-Swap (Times)	Throughput (t/h)	Gain (%)	Type	Charging Power (C)
0	–	11.55	0.00	–	317.81	0.00	Diesel	Baseline
0	0	10.39	0.67	2	353.25	11.18	Electric	0.55 C
15	0	10.06	0.33	1	364.96	14.86	Electric	0.55 C
	5	10.39	0.67	1	353.25	11.18	Electric	0.55 C
	10	10.39	0.67	0	353.25	11.18	Electric	0.55 C
20	0	10.06	0.33	1	364.96	14.86	Electric	0.55 C
	5	10.06	0.33	0	364.96	14.86	Electric	0.55 C
	10	10.39	0.67	0	353.25	11.18	Electric	0.55 C
26.5	0	9.73	0.00	0	**377.46**	**18.77**	Electric	0.55 C
	5	10.06	0.33	0	364.96	14.86	Electric	0.55 C
	10	10.39	0.67	0	353.25	11.18	Electric	0.55 C
15	0	10.06	0.33	1	**364.96**	14.86	Electric	0.5 C
	5	10.39	0.67	1	353.25	11.18	Electric	0.5 C
	10	10.73	1.00	1	342.28	7.73	Electric	0.5 C
20	0	10.06	0.33	1	**364.96**	14.86	Electric	0.5 C
	5	10.39	0.67	1	353.25	11.18	Electric	0.5 C
	10	10.39	0.67	0	353.25	11.18	Electric	0.5 C
26.5	0	10.06	0.33	1	**364.96**	14.86	Electric	0.5 C
	5	10.06	0.33	0	**364.96**	14.86	Electric	0.5 C
	10	10.39	0.67	0	353.25	11.18	Electric	0.5 C

under specific configurations, the vehicle can operate continuously without incurring additional waiting times or operational interruptions.

Nevertheless, despite these promising outcomes, this analysis alone is insufficient to conclude that a dedicated optimization framework is necessary. This limitation arises because the preliminary analysis is based on aggregate performance indicators and does not capture how route-to-route stochastic variability interacts with sequencing constraints over the full production horizon. A deeper understanding of the operational dynamics is therefore required before such a claim can be substantiated.

For this reason, Figure 3 provides further insight into the system's operational behavior. It compares the base case without trolley assistance with a configuration including a 26.5 m trolley rail operating at a charging rate of $0.5C$ (241 kW). In the trolley-assisted case, certain routes exhibit net energy regeneration rather than net energy consumption, particularly in the right-hand portion of the distribution. In addition, the box plots reveal marked route-dependent variability, highlighting the inherent dispersion in energy requirements across operating conditions.

The variability observed in Figure 3 arises from multiple sources. First, it reflects route-dependent variability in driving behavior, as observed in operational data, including variations in velocity and acceleration profiles. This component is present in the base case without trolley assistance. Second, when the trolley is introduced, the duration of the electrified segment depends on the vehicle's velocity and acceleration along the section. Consequently, variations in these conditions affect the time spent under the trolley line and, therefore, the amount of energy injected into the system. In addition, the exact moment of connection to the trolley line is inherently uncertain, as neither manual nor automated connection systems can ensure a perfectly consistent engagement point. This further contributes to variability in the effective charging duration. Together, these effects amplify the variability observed in the base case, resulting in a greater dispersion of energy outcomes across routes.

It is important to note that the reported distributions are obtained via Monte Carlo simulation and may therefore exhibit slight variation across realizations. However, using a sufficiently large number of simulations (1000 runs) mitigates this effect, ensuring that the resulting distributions provide a robust representation of the system's stochastic behavior. This variability suggests that static or heuristic strategies may fail to fully capture the complexity of real underground operations under TAS.

When this behavior is considered together with operational

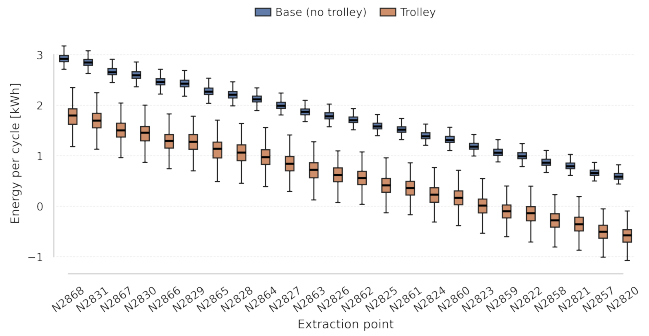

Figure 3. Energy consumption per route for the front battery under the base case (no trolley assistance) and with a trolley rail length of 26.5 m operating at a charging rate of $0.5C$ (241 kW).

constraints that prevent vehicles from repeatedly traversing the same routes, the limitations of non-optimized operational strategies become evident. In particular, route-to-route variability can introduce non-trivial operational constraints that are not adequately captured by heuristic or static approaches. This observation highlights the importance of adopting optimization-based strategies that explicitly account for route-dependent energy characteristics and the intrinsic variability of mining operations.

4.3. Optimization Results

Section 4.2 showed that route energy consumption is highly variable and depends on both route choice and the time spent under the trolley line. As a result, a fixed operating sequence may lead to unnecessary idle charging or battery swaps. To evaluate whether an optimization-based operating strategy can recover this lost performance, two fixed trolley configurations are analyzed under uncertainty. For each configuration, route energy consumption is represented through five percentile-based scenarios (10th, 30th, 50th, 70th, and 90th percentiles), which provide a compact uncertainty set spanning favorable, representative, and demanding operating conditions. The objective is to determine whether optimized route selection and charging decisions can maintain feasible full-day operation and reduce idle time without increasing trolley length.

Two cases are considered. In the first case, the trolley length and charging power are fixed at 20 m and 0.5 C (241 kW), respectively. In the second case, the trolley length remains fixed at 20 m, while the charging power is increased to 0.55 C (265.1 kW), consistent with the configurations presented in Table 2. These cases were selected because they represent challenging operating conditions in which uninterrupted full-day operation is not directly guaranteed by the preliminary analysis, unlike the 26.5 m and 0.55 C configuration. Therefore, they provide a suitable basis for quantifying how much operational improvement can be obtained through optimization alone, without modifying the trolley infrastructure.

The system comprises two batteries, located at the front and rear of the vehicle. Therefore, the charging strategy is constrained to operate at equivalent C-rates for both packs. Assigning the full charging power to a single battery is not considered feasible, as it would accelerate imbalance and uneven degradation, thereby compromising the long-term performance of the energy storage system.

Figure 4 shows the expected SoE trajectory across all scenarios, together with the uncertainty bands corresponding to the best- and worst-case conditions. The results indicate that the vehicle is able to maintain the SoE above the 20% threshold, thereby reducing exposure to deep-discharge operating conditions. Moreover, as observed in the Figure, the difference between the two batteries is negligible, suggesting that the energy management strategy can balance their utilization to some extent. This prevents one battery from being systematically used more heavily than the other, thereby improving the achievable operational autonomy.

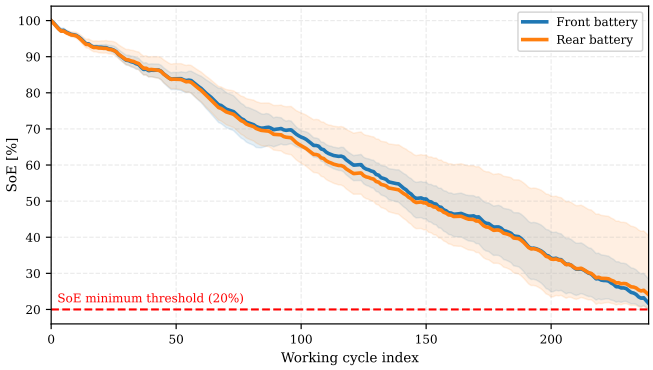

Figure 4. Expected trajectories of the SoE for the front and rear batteries for trolley length of 20 m and trolley power of $0.5C$. The envelope represents the best-case scenario (Scenario 1) and the worst-case scenario (Scenario 5). The trajectories are indexed by the work cycle, i.e., by the cumulative number of load–haul–dump cycles to be completed.

Furthermore, Figure 5 indicates that the waiting time beyond the allowable dumping window is significantly reduced compared with the non-optimized case. For the representative case, namely Scenario 3 (50th percentile), the idle time is reduced by approximately 64%, which translates into a 4.7% increase in throughput. The comparison is made against the corresponding non-optimized baseline for the same 20 m, 0.5 C configuration, in which no additional battery swap is required, but an idle time of 0.67 h is still incurred. Minor discrepancies with Table 2 may arise because Scenario 3 represents the median of the energy-consumption distribution, whereas the preliminary analysis in Table 2 is based on average values; however, these differences are expected to be small.

It is important to note that although Scenario 4 (70th percentile) exceeds the battery-swap threshold by approximately 0.1 h, it corresponds to a high-energy-consumption condition. Accordingly, the additional idle time can be regarded as an acceptable operational trade-off to avoid performing a battery swap.

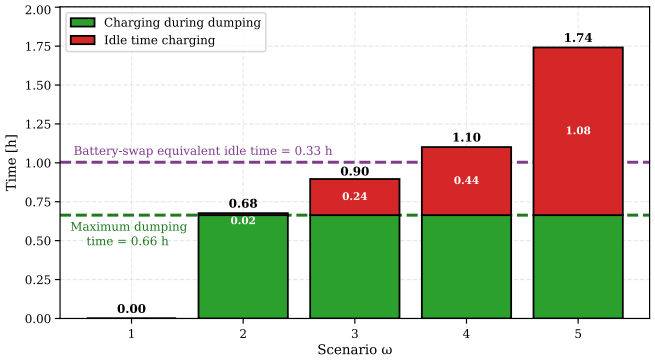

Figure 5. Total time spent on charging for trolley length of 20 m and trolley power of $0.5C$. The time is divided into two components: the first corresponds to the charging time during the dumping operation, which does not affect vehicle throughput, and the second to the idle charging time, which directly reduces throughput. In addition, the battery-swap equivalence is indicated to show the point at which the accumulated idle time becomes comparable to performing a battery swap.

Figure 6 presents the SoE trajectories for the second case study, corresponding to a trolley length of 20 m and a charging power of $0.55C$. As in the previous configuration, the vehicle is able to complete the production plan without requiring a battery swap. More importantly, the uncertainty bands become narrower, indicating that higher charging power improves the system's ability to compensate for the inherent variability of the operation. In addition, the final SoE of both batteries converges to similar values, which further confirms that the TAS contributes to balancing their utilization. This mitigates the impact of uneven energy consumption between batteries and prevents it from affecting operational performance.

Furthermore, the results in Figure 7 show the same overall trend, with a further reduction in the idle time required to complete the production plan without battery swapping. In Scenario 3, the idle time is completely eliminated, yielding a performance equivalent to the best trolley configuration reported in Table 2. Relative to the corresponding non-optimized baseline, this represents a 100% reduction in idle time and an approximately 3.91% increase in throughput.

It is also worth noting that in Scenario 4 the idle time falls below the battery-swap threshold. This indicates that even under high-energy-demand conditions, the system can cope and adapt without requiring a battery replacement and without significantly compromising throughput.

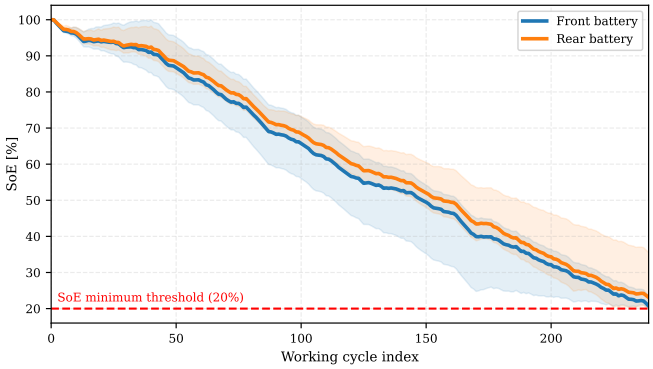

Figure 6. Expected trajectories of the SoE for the front and rear batteries for trolley length of 20 m and trolley power of $0.55C$. The envelope represents the best-case scenario (Scenario 1) and the worst-case scenario (Scenario 5). The trajectories are indexed by the work cycle, i.e., by the cumulative number of load–haul–dump cycles to be completed.

Taken together, these results indicate that an optimized routing strategy enables higher material throughput without requiring longer trolley sections. Moreover, even in the worst-case scenario, where idle time increases considerably, the system still meets the daily production target without battery swapping. This is a particularly relevant finding given the high operational variability of electric vehicles, as illustrated in Figure 3. The proposed approach, therefore, mitigates the impact of this variability and provides a reliable framework for ensuring consistent and efficient operation. In contrast, in a battery-swap-based strategy, the variability may introduce an additional swap, corresponding to an extra 0.33 h of idle time, which would significantly reduce both the practicality and the throughput of the operation.

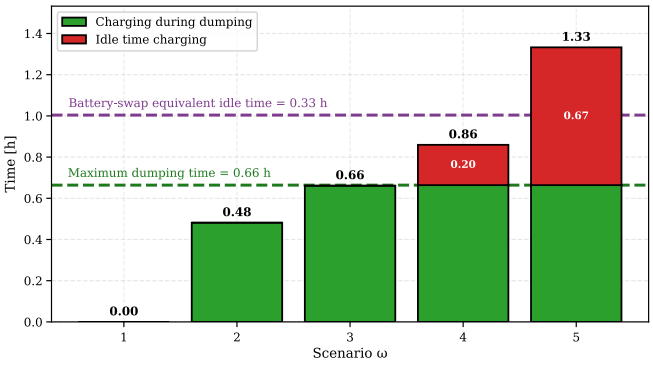

Figure 7. Total time spent on charging for trolley length of 20 m and trolley power of $0.55C$. The time is divided into two components: the first corresponds to the charging time during the dumping operation, which does not affect vehicle throughput, and the second to the idle charging time, which directly reduces throughput. In addition, the battery-swap equivalence is indicated to show the point at which the accumulated idle time becomes comparable to performing a battery swap.

In addition, the low computational time required by Gurobi (less than 5 s on an Intel i9-13900K to solve the optimization problem) suggests that the formulation can be extended to a multi-stage framework. This extension is particularly relevant because the worst-case scenarios shown in Figures 5 and 6 lie well beyond the battery-swap threshold. Although their probability of occurrence is low, in such situations a battery swap would constitute the preferred operational decision. However, explicitly enforcing this option within the current two-stage formulation would degrade the performance of the remaining scenarios, which represent the most likely operating conditions. A multi-stage approach, in which uncertainty is progressively revealed after each cycle, would enable dynamic adaptation of the operational strategy and thereby avoid this trade-off.

5. CONCLUSION

The fundamental barrier to full electrification of underground LHD fleets is that current battery technology cannot store and deliver sufficient energy to sustain a complete production shift. This work demonstrates that TAS provide a practical solution to this energy-capacity limitation by supplementing onboard battery energy through dynamic charging along electrified route segments and static connections during brief scheduled stops. The inherently stochastic nature of mining operations, driven by operational variability, changing road conditions, and evolving production requirements, necessitates adaptive real-time management of vehicle energy trajectories. In this context, the results indicate the existence of a non-trivial optimal operational solution that maximizes throughput (t/h) for a given trolley configuration while preserving the flexibility required to accommodate uncertainty.

A key contribution of this study is the formulation and application of a stochastic optimization framework to support decision-making on energy use and trolley deployment. The proposed framework enables a quantitative comparison between the preliminary analysis and the performance achieved through optimized routing and operational strategies, particularly in terms of idle time and throughput. By explicitly incorporating operational constraints and energy-balance relationships, the optimization provides insight into how trolley-assisted operation can be configured to maximize battery autonomy while ensuring feasible and efficient performance. In this sense, the optimization model serves not only as a tool to improve operational performance but also to clarify the role of trolley assistance in mitigating the effects of inherent variability in electromobility for mining applications. Equivalently, the framework can be regarded as an operational health-management layer for battery-electric fleets, in which the SoE trajectory acts as a proxy health indicator that ties condition awareness to routing and charging decisions, keeping the battery within safe operating bounds while sustaining production.

Moreover, the explicit consideration of multiple vehicle trajectories shows that, even under worst-case operating conditions, the vehicle can meet the daily production target without requiring a battery swap. Compared with battery-swapping strategies, TAS can achieve comparable or superior autonomy at lower capital cost and with higher equipment availability, because it avoids the need for duplicate battery packs and reduces downtime associated with battery replacement. Although a swap may in some cases reduce total idle time, TAS avoids these costs while still ensuring feasible operation. In this context, battery degradation is critical, as low-probability worst-case scenarios may become more restrictive as the battery ages. Consequently, incorporating such scenarios into the optimization framework is essential to ensure robust and reliable performance over the vehicle's lifetime.

For future work, it is important to incorporate more detailed battery-condition indicators, such as SoC and State of Maximum Power Available (SoMPA), to more accurately represent battery behavior under the high-power demands of this application. In addition, extending the optimization framework to explicitly include trolley rail length and power as decision variables would further enhance the applicability and practical relevance of the proposed approach. The inclusion of battery State of Health (SoH) is also necessary to evaluate the impact of prolonged trolley usage on battery degradation and to quantify the potential benefits of trolley assistance in mitigating operational limitations associated with low SoH.

Finally, a more rigorous treatment of uncertainty is required. In the present study, the number of LHD working cycles is assumed to be fixed; however, under real operating conditions, extracted tonnage is not constant, and extraction points are not always available, as mining conditions affect their operability. This may alter the sequence in which extraction points are visited and, consequently, the vehicle energy trajectory and charging opportunities. These aspects suggest that a multi-stage optimization framework may be required to fully exploit the potential of TAS, particularly given the low computational times observed in this study. In addition, exploring alternative driving policies and their trade-offs with trolley-assisted operation is an important direction for future research, as different control strategies may significantly influence both energy consumption and the effectiveness of in-motion charging, consistent with the observed trends.

ACKNOWLEDGMENT

This work was supported in part by ANID FONDECYT 1250036, Advanced Center for Electrical and Electronic Engineering, ANID Basal Project CIA250006. The authors acknowledge the support of CODELCO through the collaborative research project under which this work was developed. The first author also gratefully acknowledges the financial support of the PIENSA MINERÍA scholarship. In addition,

the first author would like to express their sincere gratitude to the Department of Electrical Engineering of the University of Chile for the financial support provided through the 2026 scholarship program for participation as a presenter in international conferences. The work of Jorge E. García Bustos has been supported by ANID-PFCHA/Doctorado Nacional/2022-21221213.

NOMENCLATURE

BEV	Battery-Electric Vehicle
BSS	Battery Swapping Station
DCFC	DC Fast Charging
DTW	Dynamic Time Warping
LHD	Load-Haul-Dump
MILP	Mixed-Integer Linear Program
PHM	Prognostics and Health Management
SoC	State of Charge
SoE	State of Energy
SoH	State of Health
SoMPA	State of Maximum Power Available
TAS	Trolley-Assisted System
UFC	Ultra-Fast Charging

REFERENCES

Ahmad, F., Saad Alam, M., Saad Alsaidan, I., & Shariff, S. M. (2020). Battery swapping station for electric vehicles: opportunities and challenges. *IET Smart Grid*, *3*(3), 280–286. doi: https://doi.org/10.1049/iet-stg.2019.0059

Alhazmi, Y. A. (2025). Electric vehicle battery swap stations: an overview and critical review. *Journal of Umm Al-Qura University for Engineering and Architecture*, 1–14. doi: https://doi.org/10.1007/s43995-025-00215-z

Bao, H., Knights, P., Kizil, M., & Nehring, M. (2024). Energy consumption and battery size of battery trolley electric trucks in surface mines. *Energies*, *17*(6), 1494. doi: https://doi.org/10.3390/en17061494

Bao, H., Knights, P., Kizil, M., & Nehring, M. (2025). Performance evaluation of alternative configurations of battery electric mining haul trucks. *IEEE Access*. doi: https://doi.org/10.1109/ACCESS.2025.3588871

Gleisner, L., García, J., Masserano, B., Troncoso, D., Jaramillo, F., Silva, J., et al. (2025). Stochastic Modeling of Electric LHD in Underground Mining to Generate Synthetic Driving Profiles. In *12th international congress on automation, robotics, and digitalization in mining* (p. 3).

Global Mining Guidelines Group (GMG). (2022). *Recommended practices for battery electric vehicles in underground mining* (Guideline). Ormstown, Quebec, Canada: Global Mining Guidelines Group. (Battery Electric Vehicles v3; Electric Mine Working Group)

Guzzella, L., & Sciarretta, A. (2007). *Vehicle propulsion systems: Introduction to modeling and optimization*. Springer. doi: https://doi.org/10.1007/978-3-642-35913-2

Halim, A. (2017). Ventilation requirements for diesel equipment in underground mines: Are we using the correct values? In *16th north american mine ventilation symposium.* Golden, Colorado, USA: Society for Mining, Metallurgy and Exploration (SME).

He, H., Zhang, Y., Xiong, R., & Wang, C. (2015). A novel Gaussian model based battery state estimation approach: State-of-Energy. *Applied Energy*, *151*, 41–48. doi: https://doi.org/10.1016/j.apenergy.2015.04.062

Hooli, J., & Halim, A. (2025, 2). Battery electric vehicles in underground mines: Insights from industry. *Renewable and Sustainable Energy Reviews*, *208*, 115024. doi: https://doi.org/10.1016/j.rser.2024.115024

Hooli, J., Skawina, B., Halim, A., & Sundqvist, F. (2024, 12). Analysing battery swapping of battery electric load haul dump (LHD) machines in block cave mining using discrete event simulation (DES). *Mining, Metallurgy & Exploration*, *41*(6), 2877-2890. doi: https://doi.org/10.1007/s42461-024-01146-4

Larminie, J., & Lowry, J. (2012). *Electric vehicle technology explained* (2nd ed.). Wiley. doi: https://doi.org/10.1002/9781118361146

Liu, X., Wu, J., Zhang, C., & Chen, Z. (2014). A method for state of energy estimation of lithium-ion batteries at dynamic currents and temperatures. *Journal of Power Sources*, *270*, 151–157. doi: https://doi.org/10.1016/j.jpowsour.2014.07.107

Mojlish, S. A. K., Sutanto, D., & Muttaqi, K. M. (2025). Impacts of ultra-fast charging of electric vehicles on power grids: State-of-the-art technologies, case studies, and a proposed improvement using a solid-state transformer. *Journal of Energy Storage*, *107*, 114913. doi: https://doi.org/10.1016/j.est.2024.114913

Muttaqi, K. M., Isac, E., Mandal, A., Sutanto, D., & Akter, S. (2024). Fast and random charging of electric vehicles and its impacts: State-of-the-art technologies and case studies. *Electric Power Systems Research*, *226*, 109899. doi: https://doi.org/10.1016/j.epsr.2023.109899

Pacejka, H. B. (2005). *Tire and vehicle dynamics* (2nd ed.). Butterworth-Heinemann.

Paraszczak, J., Svedlund, E., Fytas, K., & Laflamme, M. (2024, 1). Electrification of loaders and trucks – a step towards more sustainable underground mining. *RE&PQJ*, *12*(1). doi: https://doi.org/10.24084/repqj12.240

Rozas, H., Troncoso-Kurtovic, D., Ley, C. P., & Orchard, M. E. (2021). Lithium-ion battery State-of-Latent-Energy (SoLE): A fresh new look to the problem of

energy autonomy prognostics in storage systems. *Journal of Energy Storage*, *40*, 102735. doi: https://doi.org/10.1016/j.est.2021.102735

Sarker, M. R., Pandžić, H., & Ortega-Vazquez, M. A. (2014). Optimal operation and services scheduling for an electric vehicle battery swapping station. *IEEE Transactions on Power Systems*, *30*(2), 901–910. doi: https://doi.org/10.1109/TPWRS.2014.2331560

Sawant, V., & Zambare, P. (2024). DC fast charging stations for electric vehicles: A review. *Energy Conversion and Economics*, *5*(1), 54–71. doi: https://doi.org/10.1049/enc2.12111

Souza, E. D. (2015, 11). Improving the energy efficiency of mine fan assemblages. *Applied Thermal Engineering*, *90*, 1092-1097. doi: https://doi.org/10.1016/j.applthermaleng.2015.04.048

Valenzuela Cruzat, J., & Valenzuela, M. A. (2018). Modeling and evaluation of benefits of trolley assist system for mining trucks. *IEEE Transactions on Industry Applications*, *54*(4), 3971-3981. doi: https://doi.org/10.1109/TIA.2018.2823261

Vani, B. V., Kishan, D., Ahmad, M. W., & Reddy, B. N. K. (2024). An efficient battery swapping and charging mechanism for electric vehicles using bat algorithm. *Computers and Electrical Engineering*, *118*, 109357. doi: https://doi.org/10.1016/j.compeleceng.2024.109357

Wei, L., Liu, Q., Liu, B., & Feng, Y. (2025). Optimal economic sizing of energy storage system for trolley assisted battery electric mining haul truck considering battery degradation. *Journal of Cleaner Production*, *524*, 146452. doi: https://doi.org/10.1016/j.jclepro.2025.146452

Wu, H. (2021). A survey of battery swapping stations for electric vehicles: Operation modes and decision scenarios. *IEEE Transactions on Intelligent Transportation Systems*, *23*(8), 10163–10185. doi: https://doi.org/10.1109/TITS.2021.3125861

Zentani, A., Almaktoof, A., & Kahn, M. T. (2024). A comprehensive review of developments in electric vehicles fast charging technology. *Applied Sciences*, *14*(11), 4728. doi: https://doi.org/10.3390/app14114728

Zhao, L., Li, K., Zhao, W., Ke, H.-C., & Wang, Z. (2022). A sticky sampling and Markov state transition matrix based driving cycle construction method for EV. *Energies*, *15*(3). doi: https://doi.org/10.3390/en15031057